Molecular Therapy
Methods & Clinical Development
Original Article

Intrathecal delivery of a bicistronic AAV9 vector expressing β-hexosaminidase A corrects Sandhoff disease in a murine model: A dosage study

Alex E. Ryckman,[1] Natalie M. Deschenes,[1] Brianna M. Quinville,[1] Karlaina J.L. Osmon,[1] Melissa Mitchell,[4] Zhilin Chen,[2] Steven J. Gray,[3] and Jagdeep S. Walia[1,2,4]

[1]Centre for Neuroscience Studies, Queen's University, Kingston, ON K7L 3N6, Canada; [2]Department of Biomedical and Molecular Sciences, Queen's University, Kingston, ON K7L 3N6, Canada; [3]Department of Pediatrics, University of Texas Southwestern Medical Center, Dallas, TX 75390, USA; [4]Medical Genetics/Departments of Pediatrics, Queen's University, Kingston, ON K7L 2V7, Canada

The pathological accumulation of GM2 ganglioside associated with Tay-Sachs disease (TSD) and Sandhoff disease (SD) occurs in individuals who possess mutant forms of the heterodimer β-hexosaminidase A (Hex A) because of mutation of the *HEXA* and *HEXB* genes, respectively. With a lack of approved therapies, patients experience rapid neurological decline resulting in early death. A novel bicistronic vector carrying both *HEXA* and *HEXB* previously demonstrated promising results in mouse models of SD following neonatal intravenous administration, including significant reduction in GM2 accumulation, increased levels of Hex A, and a 2-fold extension of survival. The aim of the present study was to identify an optimal dose of the bicistronic vector in 6-week-old SD mice by an intrathecal route of administration along with transient immunosuppression, to inform possible clinical translation. Three doses of the bicistronic vector were tested: 2.5e11, 1.25e11, and 0.625e11 vector genomes per mouse. The highest dose provided the greatest increase in biochemical and behavioral parameters, such that treated mice lived to a median age of 56 weeks (>3 times the lifespan of the SD controls). These results have direct implications in deciding a human equivalent dose for TSD/SD and have informed the approval of a clinical trial application (NCT04798235).

INTRODUCTION

GM2 gangliosidosis is a family of lysosomal storage disorders (LSDs) that manifest as a result of deficient levels of functional β-hexosaminidase A (Hex A), a heterodimer composed of α- and β-subunits. This group of diseases consists of three fatal monogenic disorders, each affecting a component of the Hex A/GM2 activator protein (GM2AP) complex: Tay-Sachs disease (TSD) (*HEXA* gene, α-subunit), Sandhoff disease (SD) (*HEXB* gene, β-subunit), and GM2AP deficiency (*GM2A* gene, GM2AP). Normally, the enzyme complex works together to hydrolyze the terminal *N*-acetyl-galactosamine (GalNac) residue from GM2 ganglioside (GM2) in the lysosome of the neuron. However, if any of the previously mentioned genes possess disease-causing mutations, GM2 accumulates to pathological levels, especially within the CNS. This pathology presents in patients as rapid neurological decline culminating in death by age 4 in its most severe phenotype.[1]

As of 2023, there have been no approved therapies to slow or stop the progression of GM2 gangliosidosis. Although therapies such as substrate reduction therapy (miglustat),[2,3] pharmacological chaperone (pyrimethamine),[4,5] and enzyme replacement therapy[6,7] have all demonstrated preclinical efficacy in animal models of GM2 gangliosidosis, these therapies fell short of clinical efficacy endpoint targets and provided limited patient benefit.[8–14]

Gene therapy (GT) is a strong therapeutic candidate for GM2 gangliosidosis patients.[15–23] In this technique, functional *HEXA* and/or *HEXB* genes are packaged into a viral vector and strategically delivered to the patient for restoration of Hex A activity. Preclinical studies have demonstrated adeno-associated virus (AAV) vectors as an optimal choice for GM2 gangliosidosis because of their low immunogenicity and high levels of transgene expression within brain tissue.[24] In 2006, Cachón-González et al.[16] intracranially co-administered separate AAV2-*HEXA* and AAV2-*HEXB* vectors to SD mice. As a result, SD mice were seen to have widespread vector distribution, a significant increase in Hex A activity, and reduced GM2 accumulation within the CNS. In addition, two clinical trials are currently investigating GT for GM2 gangliosidosis, both of which use AAV vectors (NCT04798235, NCT04669535). One clinical trial (NCT04669535) adopted to co-administer 1:1 separate AAVrh8-*HEXA* and AAVrh8-*HEXB* vectors via bilateral thalamic intraparenchymal injection and intrathecal (I.T.) infusion. This technique was seen to have some clinical benefit when administered to two infantile TSD patients.[25] Although co-administration has proved effective in preclinical studies,[16,17] this technique is limited by the need for stoichiometric

Received 10 April 2023; accepted 30 November 2023;
https://doi.org/10.1016/j.omtm.2023.101168.

Correspondence: Jagdeep S. Walia, Centre for Neuroscience Studies/Pediatrics, Queen's University, Kingston, ON K7L 3N6, Canada.
E-mail: waliaj@queensu.ca

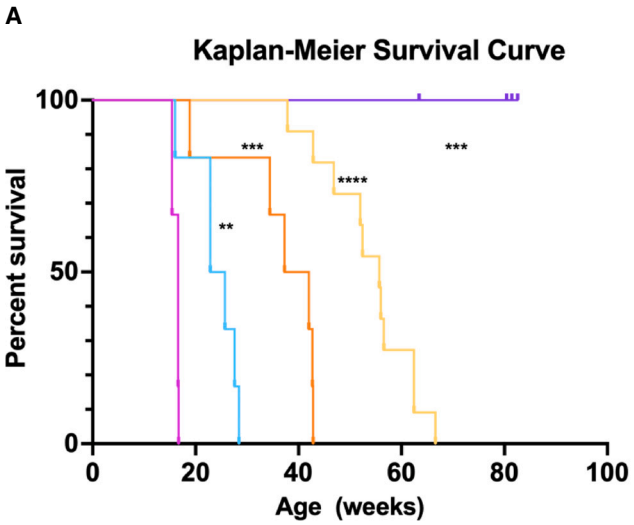

Figure 1. Kaplan-Meier survival curve of experimental doses

(A) Survival of long-term mice. Refer to the legend on the right for cohort representation. See Table S3 for study outline and details. All experimental mice were euthanized when they met the criteria for their humane endpoint (see materials and methods). Heterozygotes had a planned takedown at about 80 weeks of age. All statistics were determined on the basis of a log rank (Mantel-Cox) test. p values are as follows: low dose (LD; 0.625e11 vg/mouse) versus vehicle controls, **p = 0.0085; medium dose (MD; 1.25e11 vg/mouse) versus vehicle controls, ***p = 0.0006; high dose (HD; 2.5e11 vg/mouse) versus vehicle controls, ****p < 0.0001; and heterozygotes versus vehicle controls, ***p = 0.0006. (B) Outline of survival comparison between doses. Statistics were based on a log rank (Mantel-Cox) test.

co-infection of both *HEXA* and *HEXB* vectors for equal α- and β-subunit production and dimerization within the same cell.[15,20,26] Therefore, several bicistronic vectors carrying both *HEXA* and *HEXB* within the same cassette have been developed, mitigating the issue of co-infection.[15,20,23]

Previously, our lab performed a proof-of-concept study for our ssAAV9-*HEXB*P2A-*HEXA* bicistronic vector that demonstrated that intravenous (i.v.) administration to neonatal SD mice resulted in extension of lifespan by 60 days, improved behavioral performance, and significantly decreased GM2 accumulation compared with SD controls.[23] However, mice have been reported to possess an immature blood-brain barrier (BBB) at this age and thus may not faithfully model the human condition.[27,28] As well, i.v. injections require doses of up to 10 times that of a more CNS-directed administration such as injection into the cerebrospinal fluid (CSF).[29] Consequently, i.v. administration may also produce a higher immune response and limited CNS transduction.[30–32]

The aim of the present study was to provide further refinement of the method of administration of our bicistronic vector to inform the potential of translation to human clinical trials. Here, we have provided a proof-of-principle dose assessment and study of an I.T. route of administration via lumbar puncture (LP) for the bicistronic vector. LP represents a more localized, less invasive, and more translatable method of delivery for human patients. The bicistronic vector was tested at three different doses: a low dose (LD; 0.625e11 vg/mouse), a medium dose (MD; 1.25e11 vg/mouse), and a high dose (HD; 2.5e11 vg/mouse). Mice received immunosuppression beginning at 5 weeks of age (see immunosuppression timeline in materials and methods). The bicistronic vector demonstrated a dose-response trend in most of the study parameters, with the HD providing the greatest therapeutic benefit to SD mice. The results of this study have not only confirmed the *in vivo* efficacy of the bicistronic vector but also provided insight for the choice of human equivalent doses for a subsequent phase I/II clinical trial using this bicistronic vector, which is currently under way (NCT04798235).

RESULTS

Survival

The Kaplan-Meier survival curve of the experimental dose SD mice can be seen in Figure 1. The lifespan of all bicistronic vector-treated mice (LD, MD, and HD) was significantly increased compared with the *Hexb* knockout (KO) vehicle controls after a log rank (Mantel-Cox) statistical test. The survival curve illustrated a dose-response effect whereby the HD of the vector increased survival the most, followed by the MD and LD. The HD mice illustrated the most significant increase in survival compared with the vehicle controls, with median survival of 55.71 weeks and a range of 41.86–66.57 weeks of age. The vehicle-treated mice had median survival of 16.57 weeks and a range of 15–16 weeks. The MD also exhibited a significant increase in survival compared with the vehicle controls, with median survival of 39.65 weeks and a range of 18.86–42.86 weeks. The LD significantly increased the survival compared with the vehicle controls, with median survival of 24.29 weeks and a range of 16–28.43 weeks.

Behavioral outcomes

Rotarod: Motor coordination

The motor coordination of the experimental mice was tested over their respective lifespans using an accelerating rotarod (RR) protocol. However, as the vehicle-treated mice were humanely euthanized at 16 weeks, statistics could be reported only up until the 14 week behavioral time point. As seen in Table 1, statistics that were observed to be significant ($p < 0.05$) were reported; all dosage groups were compared against both the vehicle-treated mice and heterozygotes, as well as against every other dosage group.

As seen in Figure 2, the speed (end rotations per minute [RPM]), duration (latency to fall), and distance traveled during each trial was recorded and analyzed. Generally, within the treatment cohorts,

Table 1. Statistical summary of rotarod results until 14 weeks of age

RR: end RPM	Time point (weeks of age)			
	8	10	12	14
Significance	n.s.	n.s.	Het vs. Veh: ****p < 0.0001	Het vs. Veh: ****p < 0.0001
				Het vs. MD: ***p = 0.0005
				HD vs. Veh: *p = 0.0461
RR: LTF	Time point (weeks of age)			
	8	10	12	14
Significance	n.s.	n.s.	Het vs. Veh: ****p < 0.0007	Het vs. Veh: ****p < 0.0001
				Het vs. MD: ***p = 0.0008
RR: DT	Time point (weeks of age)			
	8	10	12	14
Significance	n.s.	n.s.	Het vs. Veh: ***p < 0.0009	Het vs. Veh: ***p < 0.0003
				Het vs. MD: ***p = 0.0003

This table corresponds to the RR graphs seen in Figure 2 and summarizes the statistical significance at each behavioral time point until 14 weeks of age (the vehicle controls were humanely euthanized prior to their 16 week time point). A mixed-effects model of repeated-measures 2-way ANOVA with Tukey's multiple comparisons was used to test for statistical significance. The p values are recorded for time points and comparisons that were significant ($p < 0.05$). RR, rotarod; RPM, rotations per minute; LTF, latency to fall; DT, distance traveled, n.s., not significant; Het, heterozygote/vehicle cohort; Veh, *Hexb* knockout/vehicle control cohort; HD, *Hexb* knockout/high-dose vector-treated cohort; MD, *Hexb* knockout/medium-dose vector-treated cohort; LD, *Hexb* knockout/low-dose vector-treated cohort.

the HD mice illustrated the greatest ability on this task over the longest period of time, with their peak performance occurring at approximately 20 weeks of age. The HD mice significantly outperformed the vehicle mice at 14 weeks of age, as seen in Figure 2 and Table 1. Interestingly, the LD mice outperformed the MD mice from 10 to 14 weeks, likely because of cohort variability, but had a large reduction in speed around 16 weeks of age, matching symptom progression for this cohort (Table S1). Similar trends were paralleled in the other parameters, as seen in Figure 2.

Open field test: General locomotion

We also tested the general locomotion of the mice with an open field test (OFT). However, the mixed-effects model of repeated-measures 2-way ANOVA with Tukey's multiple comparisons revealed that none of the OFT parameters up until 14 weeks of age illustrated any significance (Figure S1). However, we should note that the treated cohorts were still able to perform the task after all the vehicle-injected mice had died. As well, there was no significant differences seen between the heterozygotes and any of the dosage mice up until 14 weeks of age.

Biochemical outcomes

Ganglioside accumulation

GM2 ganglioside storage within the middle section of the brain (MB) (see materials and methods and Figure S2 for brain-sectioning protocol) was analyzed for all experimental mice. In brief, the GM2 concentration was visualized on a thin-layer chromatography (TLC) plate, measured using densitometry, and compared against the internal control GD1a ganglioside. The ratio of GM2 to GD1a for both short-term (ST) and long-term (LT) mice can be seen in Figure 3. A dose-response effect may have occurred for the ST mice, as the HD mice had significantly less GM2 accumulation compared with not only the vehicle controls but also the LD group. The LD group illustrated similar levels of GM2 accumulation as the vehicle controls.

A dose-response effect was not observed in the LT mice, for which GM2 gangliosides were measured when they met euthanasia criteria regardless of age. For the LT mice, the LD had significantly higher GM2 accumulation than the heterozygote positive controls. However, no other significance was seen in the LT cohorts. The HD mice had more GM2 accumulation than the MD mice, although not significant. However, there was greater variability among individuals in the HD cohort, with a coefficient of variance of approximately 0.8. After comparison, the LT mice demonstrated greater GM2 accumulation than the ST mice with the exception of the LT vehicle-injected KO group. Considering that the ST time point of 16 weeks of age was similar to the median survival of the LT vehicle-injected KO mice, these 2 groups showed similar GM2 accumulation.

Hexosaminidase A activity

Hex A activity of all cohorts was measured within the brain, liver, and serum using a fluorescent assay, as previously described.[33,34] Here, the ability of the vector to produce correctly folded and functional Hex A in a dose-dependent manner was tested. As shown in Figures 4A and 4B, the MB did not demonstrate a significant increase in Hex A activity with vector treatment. As well, a dose-response pattern was not observed in the ST mice but was in the LT mice, although it was insignificant. An additional Hex A activity assay was run in the caudal section of the brain (CB) of the ST mice for confirmation of these results, seen in Figure 4C. It was found that a dose-response pattern may have occurred in these samples and therefore may demonstrate biological variance between areas of the brain and individual subjects.

The liver (Figures 4D and 4E) exhibited similar levels of Hex A activity as the brain. At 16 weeks of age, the liver may have demonstrated a dose-response effect, where the HD illustrated significantly greater Hex A activity than the vehicle controls. The LT liver Hex A activity did not exhibit a dose-response trend and the vector-treated groups had similar levels of Hex A activity at their respective endpoints.

Hex A activity was also measured within the serum of all experimental mice across their lifespan. Blood collections were taken prior to injections at 5 weeks of age, which acted as a baseline Hex A activity for comparison. The highest Hex A activity was seen for most groups at 12 weeks of age, 6 weeks after vector delivery. Two statistical analyses were performed on this set of data: comparison of groups within each time point (Table 2) and comparison of each group between time points relative to baseline (Table 3). These comparisons were made up until 16 weeks of age, when the vehicle controls reached their humane endpoint.

As seen in Table 2, at baseline, the heterozygotes had significantly higher Hex A activity than all *Hexb* KO groups. At 8 weeks of age

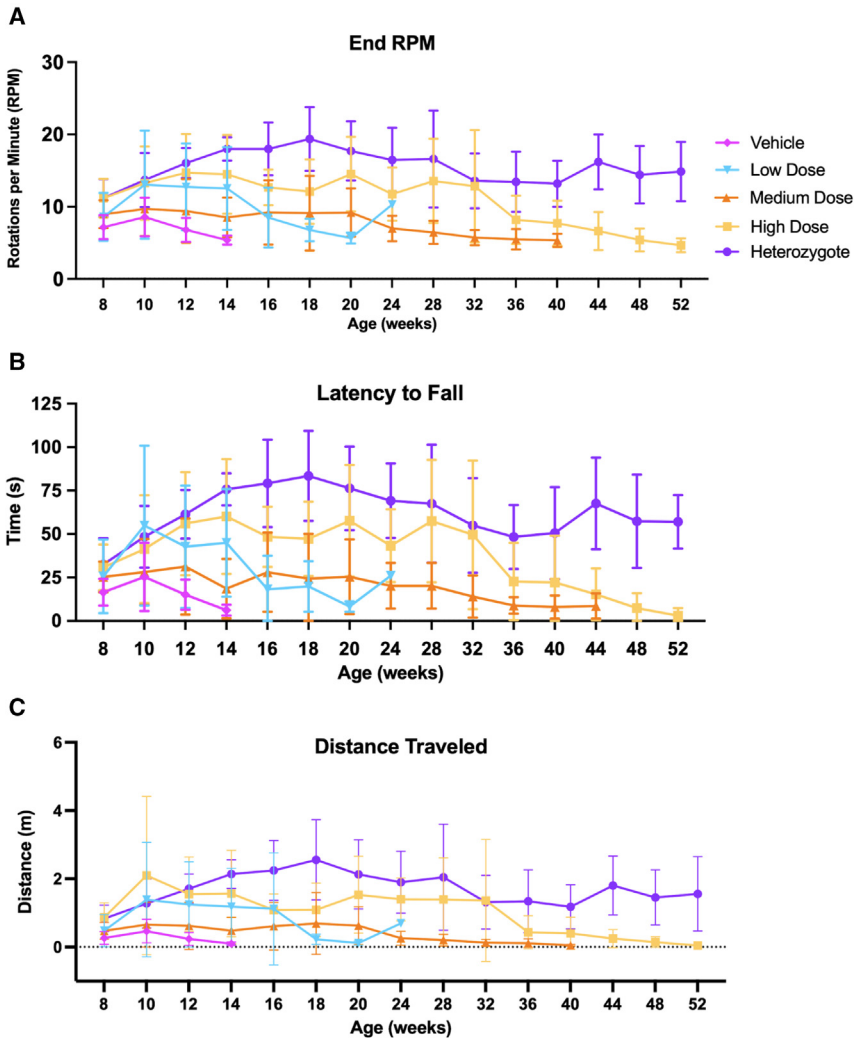

Figure 2. Motor coordination tested via rotarod across lifespan of mice

Rotarod (RR) testing was performed bi-weekly from 8 to 20 weeks of age and monthly from 24 to 52 weeks of age. See the legend at the top right for cohort representation. Each RR trial was performed in triplicate by each mouse. The statistical significance for each RR parameter up until 14 weeks is reported in Table 1. (A) RR parameter: end rotations per minute (RPM). The average speed of travel of experimental mice at the end of the RR trial at each time point across the study. (B) RR parameter: latency to fall (LTF). The average length of time which the experimental mice remain on the RR at each time point across the study. (C) RR parameter: distance traveled. The average distance the experimental mice traveled on the RR at each time point.

(2 weeks after vector injection), the heterozygotes had significantly higher Hex A activity than all groups except the HD treated mice. As well the HD mice had significantly higher activity than the vehicle group. At 12 weeks, peak Hex A activity was observed for almost all groups except the MD, who seemed to have highest activity at 28 weeks of age. All vector-treated groups had significantly higher Hex A activity compared with the vehicle controls. Lastly, at 16 weeks of age, the HD and LD group were seen to have significantly higher Hex A levels than the vehicle controls. As seen in Table 3, the greatest increase in Hex A activity from baseline was seen at 16 weeks of age. This increase was significant for the HD group and less so for the LD group, but not for the MD group.

Biodistribution of vector

The vector copy number in the gross organs and CNS of the experimental mice was assessed using qPCR with *HEXA* (bicistronic vector copy number) and *LaminB2* (regulatory gene, mouse genome copy number) primers. As seen in Figure 5A, the highest amount of vector was found within the kidney, spleen, and sections of the brain at 16 weeks. It was evident that a dose-response effect may have been observed throughout all ST tissues, where the HD provided the greatest vector copy number in all analyzed tissues except the MB. In the kidney, the HD had significantly higher vector copy numbers than the MD and LD. No other significant differences were found between doses in the remaining tissues.

The LT tissues were collected at each subject's individual humane endpoint and thus differ from the ST biodistribution by lack of a fixed endpoint. Thus a dose-response pattern was not necessarily expected, but it was observed throughout some tissues (Figure 5B). The liver had the greatest vector copy number in all of the LT tissues, with the CNS also exhibiting higher vector copy numbers. In the liver, the HD mice had significantly greater vector copy numbers than the MD and LD mice. However, no other significant differences among doses were seen in the LT tissues. The other gross organs (i.e., heart, lung, spleen, kidney, gonad, and arm muscle) had minimal vector present at the humane endpoint of the LT mice. In contrast, the CNS maintained vector until the humane endpoint, as it had very similar values to its ST counterparts. For all other LT organs, there was a clear decrease in vector copy number compared with the 16 week endpoint.

DISCUSSION

Although our initial publication described the efficacy of the ssAAV9-*HEXB*P2A-*HEXA* GT after i.v. administration of a single dose in neonatal mice, the present study greatly expands and informs the use of this vector by evaluation of escalating doses given by a different route, i.t., into 6-week-old SD mice. For most biochemical and phenotypic parameters, a dose-response relationship was observed. This effect was especially evident in the survival extension of the SD mice

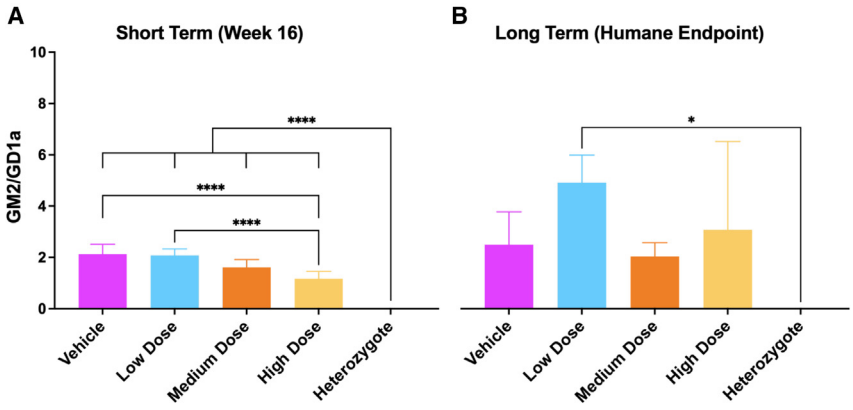

Figure 3. GM2 accumulation in the middle section of the brain

GM2 ganglioside was visualized and measured using densitometry against the internal control GD1a ganglioside in the middle section of the brain (MB). Statistical significance was tested using a 1-way ANOVA, with Tukey's multiple comparisons. (A) MB GM2 storage for the short-term mice sacrificed at 16 weeks of age. The HD had significantly less GM2 accumulation than the LD and the vehicle controls (****$p < 0.0001$ for both). As well, the heterozygotes had zero GM2 accumulation, which was highly significant in comparison with all experimental groups (****$p < 0.0001$). (B) MB GM2 storage of the long-term mice (euthanized at humane endpoint). The LD had significantly greater GM2 storage than the heterozygotes (*$p < 0.0001$).

(Figure 1); the LD increased survival by 1.5-fold, the MD by 2.4-fold, and the HD by 3.4-fold relative to the untreated vehicle controls. Of the three tested doses, the HD (2.5e11 vg/mouse) provided the greatest increase in Hex A activity, the most significant decrease in GM2 accumulation, and the largest improvements in functional benefits (i.e., extended survival and increased motor coordination). Typically, SD mice exhibit symptoms (e.g., shakiness, stiffening of body, poor locomotion, decreased body weight) at about 12–14 weeks of age[21,35,36] and drastically decline toward death at about 16 weeks of age, as seen with our vehicle controls. However, the HD delayed disease progression enough to allow mice to perform at similar levels to the heterozygotes during behavioral testing up until approximately 32 weeks of age, as seen in Figure 2. Additionally, a qualitative analysis of the LT mice (Table S1) revealed that the HD mice had a greater elapsed time between symptom onset and humane endpoints than both the MD and LD mice.

The HD of this study was chosen as a sub-maximum feasible dose for human translation.[37–40] The definition of 2.5e11 vg in a mouse by I.T. injection assumes the following: 1e14–5e14 vg/mL approaches the maximum concentration of AAV9 without risk for aggregation in this buffer formulation. If a standard I.T. injection volume of 10 mL is used and the maximal concentration of AAV9 is 5e14 vg/mL, this sets a maximum feasible human dose at 5e15 vg/patient. Mice have a CSF volume of approximately 0.035 mL, while humans have a CSF volume of approximately 140 mL, creating a 4,000-fold dosing extrapolation factor between mice and humans. With these assumptions, we extrapolate that a 1e15 vg human I.T. dose roughly equates to a 4,000-fold lower mouse dose of 2.5e11 vg, our study's chosen HD. Significant therapeutic benefit was seen with the HD in this study, although even at this dose it did not illustrate maximal efficacy (measured response plateaus). Thus, future studies should investigate an earlier treatment or a higher dose, which would be expected to increase the therapeutic benefit.

Not all LT mice exhibited a severe motor phenotype (i.e., ataxia, muscle weakness, and stiffness) but they did lose >15% of their body weight (Figure S3; Table S2). As seen in the LT data (Figure 3), toxic GM2 accumulation within non-transduced cells leading to cell death may be one explanation for early euthanasia in treated SD mice, compared with controls. Buildup of GM2 in the MB was greater for the LT mice compared with ST; however, more variability existed among individual LT mice than the ST mice. As the LT mice were assessed at their respective humane endpoints, it is not surprising that GM2 accumulated similar to the vehicle controls. It seems that treatment rescue may have been incomplete in these cases, leading to organ damage and necrosis which ultimately affected both treated and untreated cells. Thus, a higher dose or an earlier treatment may increase survival of SD mice to reach that of the heterozygote mice. Vector biodistribution was much higher at 16 weeks than at respective humane endpoints, except for the liver and CNS, which seemed to maintain high levels of vector copy numbers. It may be possible that the immune tolerance induced by rapamycin and prednisone treatment diminished over time (mice stopped receiving immunosuppression at 25 weeks of age), thus leading to immune-mediated destruction of Hex A-expressing cells.[41] However, analysis of the serum time course (Figure 4F) and behavioral testing (Figure 2) after 25 weeks of age does not indicate any drop in performance or Hex A activity levels. It is also possible that mere age had a role in symptom progression and weight loss. It is well known that older neurons accumulate impaired proteins and damaged mitochondria as a result of oxidative stress over time.[42] Perhaps as our mice aged, a reduction in neuronal tolerance of toxic pathology, such as an increased GM2 load, occurred, thus increasing their vulnerability to neurodegeneration.[43]

Only 2 of 35 treated *Hexb* KO mice presented with anomalies (i.e., enlarged spleen and calcified tissue on heart) at necropsy, both of which survived to 55 and 61 weeks of age. Five of 6 of the LT untreated heterozygotes (sacrificed at approximately 80 weeks of age) presented with enlargement of the spleen, liver, uterine horns, and thyroid. Thus, it seems likely that these sporadic anomalies are due to mouse aging rather than being treatment related. Prior studies have also shown the C57/Bl6 strain of mice to be prone to hematopoietic neoplasia with age.[44] However, it is important to note that no liver nodules were found in the treated *Hexb* mice, as observed in previous i.v. neonatal studies.[36] However, it is important to note that neonatal liver integration events affecting the *Rian* locus leading to

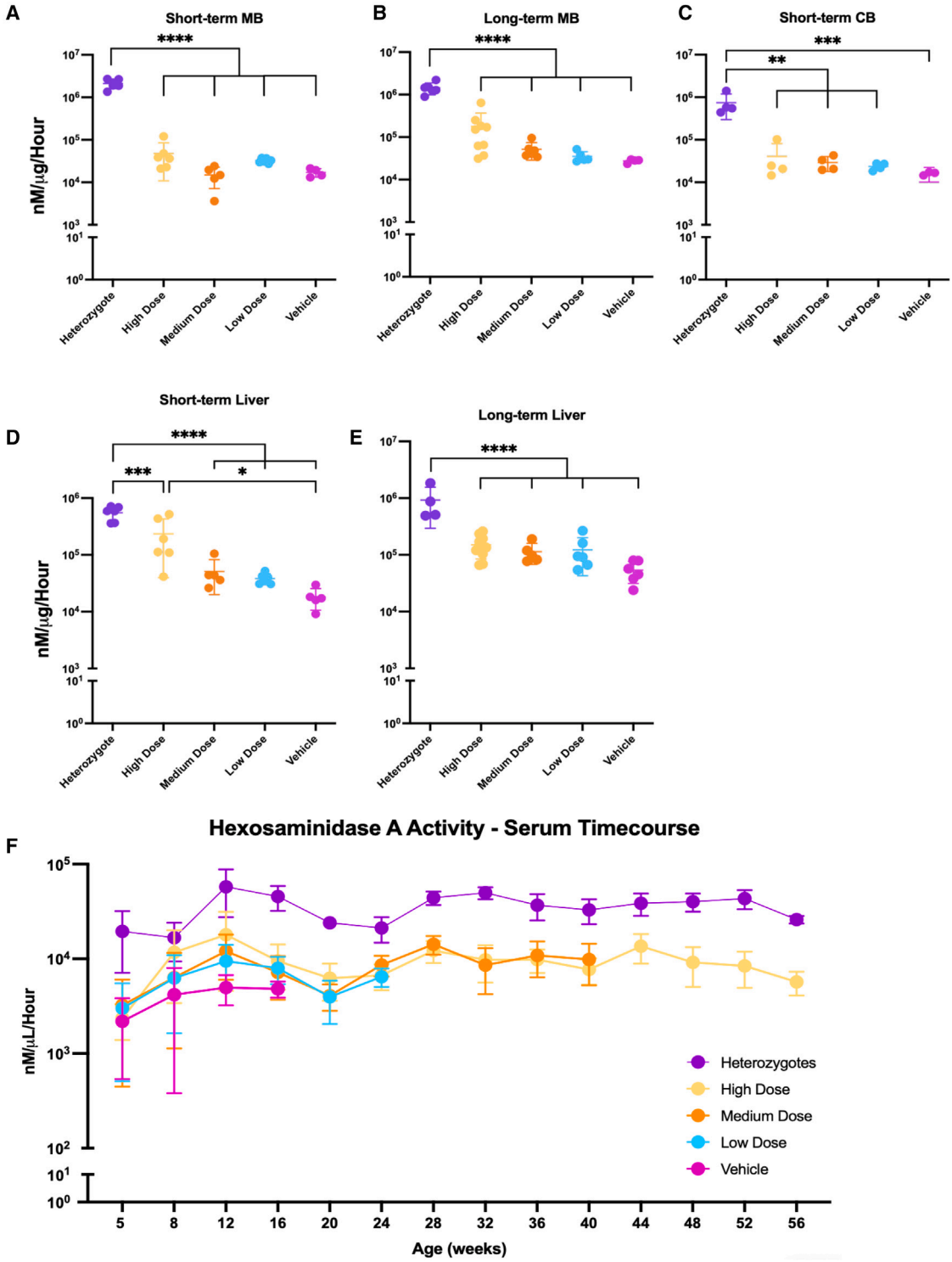

Figure 4. Summary of hexosaminidase A activity within the brain, liver, and serum

Note the logarithmic y axis scale for all graphs. All graphs illustrate the mean hexosaminidase A (Hex A) activity of each subject with SD. (A) Hex A activity within the middle section of the brain (MB) at 16 weeks of age (short-term). Hex A activity was measured by the amount of fluorescent product (4MU) produced within an hour (nM/μg protein/hour) (****$p < 0.0001$). (B) Hex A activity within the MB at respective long-term humane endpoints (****$p < 0.0001$). (C) Hex A activity within the caudal section of the brain (CB) at 16 weeks of age. The statistical summary includes Hets vs. HD, **$p = 0.0014$; Hets vs. MD, **$p = 0.0012$; Hets vs. LD, **$p = 0.0011$; and Hets vs. Veh, ***$p = 0.0009$. (D) Hex

(legend continued on next page)

hepatocellular carcinoma were the most likely cause of the liver nodules seen by Walia et al.[36,45,46] This phenomenon has not been observed with adult murine injections of AAV vectors.[47,48] Overall, there was no clear evidence of any treatment-related adverse effects in our study.

Previously, our lab performed a proof-of-concept study with a LD (2.04e10 vg/mouse) of the ssAAV9-*HEXB*P2A-*HEXA* bicistronic vector administered i.v. in neonatal SD mice.[23] Survival of these mice reached 26.57 weeks of age, which falls within the LD survival range in this study. As well, GM2 accumulation of both LDs was comparable. As of this writing, Woodley et al.[23] is the only comparable *in vivo* bicistronic study. Ornaghi et al.[20] showed promise with a lentiviral-based *HEXA/HEXB* bicistronic vector in SD fibroblasts. As well, another *HEXA/HEXB* bicistronic vector strategy has been tested in WT Wistar rats, which demonstrated significant increases in Hex A plasma levels with i.v. administration.[49] However, the efficacy of this vector has yet to be reported in SD models.

It is also important to compare our data with an alternative GT option for SD, which uses a self-complementary vector carrying *HEXM*, originally developed by Tropak et al.[22] in 2016. The *HEXM* vector was tested by our lab, where it was found that i.v. injection of neonatal SD mice increased survival from 15 weeks to a median of 40 weeks of age.[21] Interestingly, an i.v. dose of 5e10 vg/mouse increased Hex A levels and significantly decreased GM2 storage in the MB, the same as in the present study and similar to our previous studies.[21,23,50] Later, a dosage study was performed for the *HEXM* vector, where an LD (2.5e12 vg/mouse) and an HD (1e13 vg/mouse) were investigated.[50] Here, the median survival of the *HEXM* vector HD mice reached 56.7 weeks of age, thus proving its silmilar efficacy to the HD in the present study. However, 8 of 14 mice died within one month of administration of the HD of the *HEXM* vector, suggesting possible dose-related toxicity. Although the HDs in both our study and the *HEXM* study were able to extend survival approximately 3-fold that of the vehicle controls, the i.v. dose was 10 times higher than that of the I.T. dose used in our present study. Ultimately, it is difficult to directly compare these studies, as the bicistronic and *HEXM* vectors were different, and the routes of administration were different, but a lower total body dose of AAV is more desirable for a similar efficacy.

This study was not without limitations. We used a fixed dose, such that all mice, whether 15 or 21 g, received the same dose (e.g., all HD mice received 2.5e11 vg). This factor alone could account for some variability in all measured parameters, as could variability in the injections themselves, considering the technical challenge in performing lumbar I.T. injections in mice. Immunosuppression was performed via oral gavage on a daily basis until mice were 25 weeks of age. Previous studies have reported this technique to increase overall stress on mice, which could have had an impact on the study.[51–53] As well, this study could have benefited from immunological assays to check the immune response to the bicistronic vector at differing doses as a safety measure, but those measures are beyond the scope of this study. It is also worth mentioning that rapamycin and prednisone have been implicated in the pathology of LSDs previously and as such may have influenced study parameters. For example, rapamycin has been reported to increase autophagy within the cell, which may have increased clearance of the GM2 load and possibly affected the survival of our study animals.[54,55] Additionally, histological analysis was not performed in this study as it will be evaluated in a toxicology study and is beyond the scope of this study. Lastly, although GT studies typically use an empty AAV or AAV containing β-galactosidase (β-gal) cDNA as their vehicle control solution, we used a vehicle solution similar to those used in previous studies.[56,57]

Here we have confirmed the LT efficacy of the ssAAV9-*HEXB*P2A-*HEXA* vector for the treatment of GM2 gangliosidosis, as well as guided the choice of dose and route of administration for our human clinical trial, which was approved by Health Canada in 2020 (NCT04798235). The I.T. HD (2.5e11 vg/mouse; human equivalent dose of 1e15 vg) provided significant survival, behavioral, and biochemical benefit to the SD mice. However, earlier intervention or a higher dose should be investigated, as it was apparent that maximal efficacy was likely not achieved when treating mice at 6 weeks of age, even with our HD. In addition, it is possible that a combination administration (i.e., i.v. and I.T.) could allow further survival benefit than either alone and thus warrants investigation. These results can be extrapolated to TSD patients as well considering both *HEXA* and *HEXB* were delivered.

MATERIALS AND METHODS

Animal model and experimental design

The SD mouse model (C57BL/6:C129, *Hexb*$^{-/-}$) was obtained from the Jackson Laboratory, and colonies were further established through breeding at Queen's University Botterell Hall. The SD mouse model was created by inserting a neomycin cassette into exon 13 of the *Hexb* gene, resulting in production of non-functional Hex A β-subunits, a severe motor phenotype, and death by 14–16 weeks of age.[21,35,36,58] Experimental animals were obtained with KO:KO (*Hexb*$^{-/-}$:*Hexb*$^{-/-}$) and KO:heterozygote (*Hexb*$^{-/-}$:*Hexb*$^{+/-}$) crosses, and at 5 weeks of age, mice were randomly assigned to cohorts. All mice, including heterozygotes (n = 12), vector-treated *Hexb* KO mice (n = 40), and vehicle-treated *Hexb* KO mice (n = 12), were subject to a 12 h light cycle from 7 a.m. to 7 p.m., in a climate-controlled room. Each cohort was filled on the basis of mouse availability and was not evenly split into females and males. A detailed

A activity in the liver at 16 weeks of age. The statistical summary includes Het vs. HD, ***p = 0.0009; Het vs. MD/LD/Veh, ****p < 0.0001; and HD vs. Veh, *p = 0.0403. (E) Hex A activity in the liver at respective long-term humane endpoints (****p < 0.0001). (F) Hex A activity in serum across lifespan. See the legend at the bottom right. Hex A activity was measured by the amount of fluorescent product (4MU) produced per microliter of serum in an hour. Each point represents the mean activity, and the errors bars represent the SD. Hex A activity was measured up until there was a minimum of n = 3 for each cohort. Two analyses were run on the serum data: (1) a within-time-point comparison and (2) a between-time-point comparison. A statistical summary for Figure 4F can be seen in Tables 2 and 3.

Table 2. Significance summary of hexosaminidase A activity for serum time course: within-time-point comparison

	Time point (weeks of age)			
	5 (Baseline)	8 (2 weeks post-injection)	12 (Peak serum Hex A activity)	16 (Short-term endpoint)
Statistical significance	Het vs HD, *p = 0.0196 Het vs MD, *p = 0.0256 Het vs LD, *p = 0.0238 Het vs Veh, *p = 0.0184	Het vs HD, n.s. Het vs MD, *p = 0.0144 Het vs LD, *p = 0.0116 Het vs Veh, **p = 0.0026 HD vs Veh, *p = 0.03778	Het vs HD, **p = 0.0095 Het vs MD, **p = 0.0035 Het vs LD, **p = 0.0024 Het vs Veh, **p=0.0013 HD vs Veh, *p = 0.0112 MD vs Veh, *p = 0.0207 LD vs Veh, *p = 0.0457	Het vs all, ****p < 0.0001 HD vs Veh, *p = 0.0150 LD vs Veh, *p = 0.0101

This table corresponds to Figure 4F. The statistical significance of Hex A activity for all cohorts was tested using a mixed-effects model of 2-way ANOVA with Tukey's multiple comparisons. The treatment groups were compared against each other within each time point until 16 weeks of age (vehicle controls were euthanized at this time point). Hex A, hexosaminidase A; Het, heterozygote/vehicle cohort; Veh, *Hexb* knockout/vehicle control cohort; HD, *Hexb* knockout/high-dose vector-treated cohort; MD, *Hexb* knockout/medium-dose vector-treated cohort; LD, *Hexb* knockout/low-dose vector-treated cohort.

study and cohort outline can be seen in Table S3 and the outcome measures in Table S4. All experimental protocols and procedures were approved by Queen's University Animal Care Committee and run in accordance with the Canadian Council on Animal Care.

Immunosuppression via oral gavage

Oral gavage of prednisone (catalog #P6254; Sigma-Aldrich) and rapamycin (catalog #R-5000; LC Laboratories) was performed throughout the study in the attempt to reduce the immune response by creating immune tolerance to the vector.[41] Immunosuppression began at 5 weeks of age and was carried out for 20 weeks, and mice received 100 μL each day. Rapamycin was administered via oral gavage at a loading dose of 3 mg/kg on the first day of gavage and continued at a dose of 1 mg/kg. Rapamycin was not tapered. Prednisone was administered at a dose of 0.24 mg/kg/day for 10 weeks, and tapered for 5 weeks, during which the dose was reduced by 0.04 mg/kg/week.

Plasmid and vector preparations

Heterozygous (*Hexb*$^{+/-}$) and KO (*Hexb*$^{-/-}$) SD mice were used as control and experimental animals. Heterozygotes received 10 μL TMN200P vehicle (lot #082718EW-01), while experimental SD mice received varying doses of the bicistronic vector, along with 10 μL of the vehicle for the last KO cohort. The bicistronic h*B2A* plasmid and vector were constructed as previously described.[23] The vector sequence includes the cDNA of human *HEXB* and *HEXA* genes connected using a P2A self-cleaving peptide under the CAG promoter. A vector diagram can be found in Woodley et al.[23] The ssAAV9-CAG-*HEXBP2AHEXA* vector and TMN200P vehicle were obtained from the Viral Vector Core Laboratory from Nationwide Children Hospital, and the vector's certificate of analysis can be found in Figure S4.

Table 3. Significance summary of hexosaminidase A activity for serum time course: between-time-point comparison

	Time point comparison (weeks)		
Dose	5 vs. 8	5 vs. 12	5 vs. 16
HD	*p = 0.0176	*p = 0.0325	**p = 0.0047
MD	n.s.	n.s.	n.s.
LD	n.s.	n.s.	*p = 0.0273

This table corresponds to Figure 4F. The statistical significance of the hexosaminidase A activity for all cohorts was tested using a mixed-effects model of 2-way ANOVA with Tukey's multiple comparisons. Each individual treatment group's baseline activity (5 weeks) was compared with every other time point until 16 weeks of age (vehicle controls were euthanized at this time point). HD, *Hexb* knockout/high-dose vector-treated cohort; MD, *Hexb* knockout/medium-dose vector-treated cohort; LD, *Hexb* knockout/low-dose vector-treated cohort.

Vector injections

The bicistronic vector was injected at 6 weeks of age in the SD mice using an i.t. LP (protocol described below). A total volume of 10 μL was injected at varying doses: HD (2.5e11 vg/mouse, ∼1.67e13 vg/kg), MD (1.25e11 vg/mouse, ∼8.33e12 vg/kg), and LD (6.25e10 vg/mouse, ∼4.16e12 vg/kg). The control mice were injected with 10 μL of the vehicle solution.

Intrathecal LP

Experimental mice were dosed with a single i.t. injection of the bicistronic vector at 6 weeks of age (injections took place over a 12 h time window in total). A 50 μL Hamilton syringe (catalog #7637-01; Hamilton) was cleaned, autoclaved, and loaded with 10 μL vehicle or bicistronic vector solution prior to injection. In order to perform the injection, mice were first induced with 5% isoflurane and maintained at 3% isoflurane with the use of a nose cone. The hips of the mouse were placed on top of a 15 mL conical tube for better palpation of the lumbar spinal processes. The injection site was shaven with a peanut clipper (catalog #8655; Wahl Professional) and wiped with 70% ethanol for sterilization. The hips were first palpated, then the spinal process of L5 and L6 were located. The space between the spinal processes of L5 and L6 is where the 30G Hamilton needle (catalog #7803-07, point style 4, length 0.5 in, angle 12; Hamilton) was placed. The needle was inserted perpendicularly in this specific area until the needle came to a natural stop (hit bone), then the needle was tilted toward the caudal end of the spinal column at a 30° angle, where it slipped between the vertebrae into the CSF space, at which point the vector/vehicle was slowly injected into the CSF space. Successful injection was indicated by a tail flick spinal reflex as the needle punctured the dura mater. After injection, the mice were taken off isoflurane, placed in a prone position, and monitored for motor function and general recovery. At this time, mice were placed under a heat lamp to maintain body temperature.

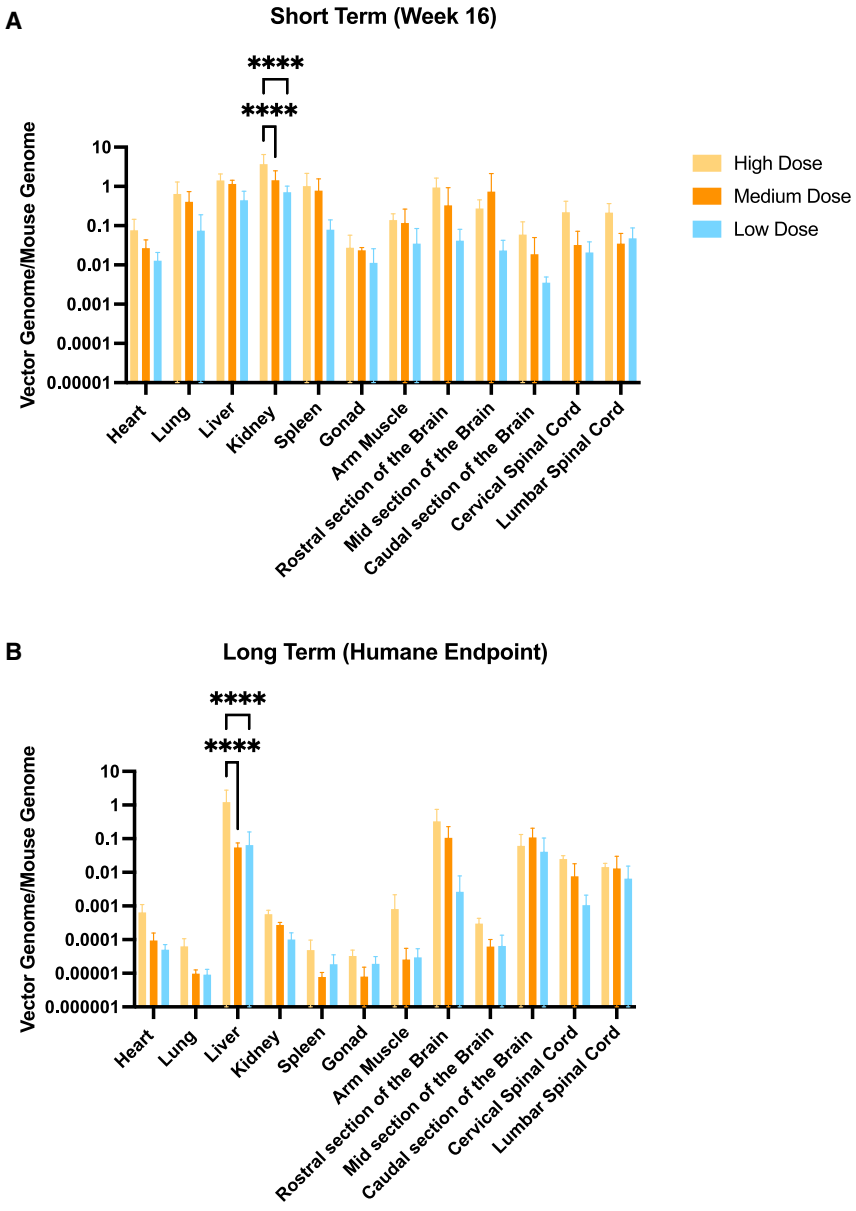

Figure 5. Bicistronic vector biodistribution

See the legend at the right for cohort representation. Note the logarithmic y axis scale. Vector copy number was measured in all gross organs and the CNS, using qPCR of *HEXA* and *LaminB2* primers. (A) Short-term vector biodistribution. Tissues were collected at 16 weeks of age. Significance was seen in the kidney between the high dose and low dose (****p < 0.0001). The high dose also had significantly greater vector copy number than the medium dose (****p < 0.0001). (B) Long-term vector biodistribution. Tissues were collected at each subject's respective humane endpoint. Significance was seen in the liver, where the high dose was significantly greater than the medium dose (****p < 0.0001) and the low dose (****p < 0.0001).

Behavioral testing

Behavioral testing began at 8 weeks of age, and was performed biweekly up until 20 weeks of age, whereupon testing was performed monthly. Behavioral testing sessions included the use of OFT to assess general locomotion, and an accelerated RR protocol to evaluate motor coordination as previously described.[59]

Tissue/serum collection and processing

Tissue samples were collected at the 16 week ST endpoint as well as the LT humane endpoints for all mice. The humane endpoint was defined by 15% weight loss from the peak recorded weight, a body condition score of 2 or lower, or by the inability to right itself from a supine position. All mice were euthanized by CO_2 asphyxiation and cardiac puncture to follow. Next, cardiac perfusion was performed using 10 mL room-temperature 1× PBS. Samples from visceral organs were collected including the heart, lungs, liver, kidney, spleen, gonads, and bicep. Additionally, samples were collected from the lumbar and cervical spinal cord, and the rostral brain, MB, and CB. Each organ was divided for qPCR vector quantification and biochemical analysis. These sections were frozen and stored at −20°C. The sectioning strategy of the brain can be seen in Figure S2.

Starting at 5 weeks of age (baseline), monthly blood collections were taken at 8, 12, 16, 20, and 24 weeks of age, continuing every 4 weeks, up until and including the age of euthanasia of the mouse. Each mouse was placed in a restraining tube and the injection site of the right hind-leg was shaved, swabbed with 70% ethanol, and smeared with petroleum jelly. The saphenous vein was poked with a 26G needle and approximately 150 μL of blood was collected using a capillary Microvette tube (catalog #KMIC-SER; Kent Scientific). The blood was centrifuged at 3,500 rpm for 10 min. Serum was collected and stored at −20°C until ready for assay.

Ganglioside storage assay

GM2 gangliosides were extracted according to previously determined protocols.[23,60,61] In brief, frozen MB samples were submerged in 700 μL 1× PBS, sonicated with three 10 s pulses at an amplitude of 20%, and centrifuged at 13,300 rpm and 4°C for 20 min. The supernatant was collected, and 400 μL was aliquoted for the MB hexosaminidase assay. The remaining supernatant and pellet were used for the GM2 storage assay.

Gangliosides were extracted from the MB with methanol and chloroform solvents, isolated using column chromatography, and then separated on a TLC plate (55 mL:45 mL:10 mL chloroform/methanol/0.2% $CaCl_2$ mobile phase). The TLC plates were doused with orcinol in 10% sulfuric acid and dried at 120°C for visualization of bands. Densitometry analysis was performed on each plate with ImageJ

software after a picture was taken of the plates. Total gangliosides, GM2 gangliosides, and GD1A gangliosides (internal control) intensity was measured. The GM2/GD1A ratio was used to quantify GM2 accumulation in the MB as an indicator of disease progression and therapy effectiveness.

Hexosaminidase assay

Total hexosaminidase and Hex A isoenzyme activity was measured using previously described protocols.[33,34] The serum/cell lysate was incubated at 52°C instead of 42°C–44°C. Hexosaminidase activity was measured in the serum over the lifespan of each mouse, along with the endpoint MB, CB, and liver samples. Serum samples were diluted 1:35 in citrate phosphate (CP) buffer. The 4-methylumbelliferyl-2-acetamido-2-deoxy-β-D-glucopyranoside (4-MUG) (catalog #M334000; Toronto Research Chemicals) substrate was used for the total hexosaminidase assay. For Hex A activity specifically, 1/3 of the diluted serum sample was heat-inactivated at 52°C for 2 h to inactivate the Hex A enzyme leaving Hex B as a result. The heat-inactivated (HI) samples also received 4-MUG substrate. To calculate the Hex A activity alone, the HI sample's activity was subtracted from the total hex activity (4-MUG). Additionally, β-gal activity was measured using 4-methylumbelliferyl-β-D-galactopyranoside (MUGal) (catalog #M1633; Millipore Sigma) substrate as an internal control. Serum samples were incubated at 37°C in a 3.2 mM MUG/MUGal substrate solution for one hour. Enzyme activity was stopped with 0.1 M 2-amino-2-methyl-1-propanol (AMP). The assay was visualized using the fluorescent breakdown product (4MU), at an excitation wavelength of 365 nm and an emission wavelength of 450 nm. Results from the 4-MUG assays were compared with a 4-methylumbelliferone (4-MU) standard curve which ranged from 130000 to 0.73 nM. The hexosaminidase assay was performed with the same protocol for the MB, CB, and liver samples. Samples were diluted 1:35, 1:35, and 1:200 in CP buffer for the MB, CB, and liver, respectively. A bicinchoninic acid (BCA) assay (catalog #23225; Thermo Fisher Scientific) was performed to quantify the total amount of protein present in the MB, CB, and liver samples and was used for comparison with the Hex A activity levels.

Vector biodistribution qPCR analysis

All gross organs, spinal cord, and brain samples collected from mice were analyzed for vector biodistribution by assessing the number of viral genomes per mouse genome. Genomic DNA was extracted from each organ using a gSYNC DNA Extraction Kit (catalog #GS100; Geneaid) and the copy number of the bicistronic vector was then determined using qPCR. Vector copy number was determined from the mean *HEXA* Ct value (viral genome) compared with the mean Ct value of the regulatory gene LaminB2 (mouse genome). All qPCRs were accomplished using PowerUp SYBR Green Master Mix (catalog #A75242; Thermo Fisher Scientific) on the Applied Biosystems 7500 Real-Time PCR System. The human *HEXA* primers used for the viral quantification include 5′-TATGG CAAGGGCTATGTGGT-3′ (forward) and 5′-TGATTGTGTCTGG CTGAATCTT-3′ (reverse). The regulatory gene LaminB2 primers used for mouse genomic DNA quantification include 5′-GGACCCA AGGACTACCTCAAGGG-3′ (forward), and 5′-AGGGCACCTCCA TCTCGGAAAC-3′ (reverse).

Statistical analysis

All statistical analyses were performed using GraphPad Prism version 8. For behavioral testing, a repeated-measures 2-way ANOVA (with a mixed-effects model because of missing values) with Tukey's multiple comparisons was performed to compare dose groups versus a motor parameter across all time points. Repeated-measures ANOVA cannot be performed if values are missing, which occurs in later time points as mice reach their humane endpoint, so a mixed-effects model was used. Behavioral analysis was performed until each cohort had 3 mice surviving, and the last recorded behavioral time point was at 52 weeks of age. Three parameters (i.e., distance traveled, mean speed without rest, and resting time in the zone) for OFT were measured during one 5 min testing period for each mouse during each time point. Each parameter was analyzed individually and the mean and SD were recorded. As well, three parameters were recorded for RR (i.e., end RPM, distance traveled, and latency to fall) for each mouse during each trial. Three trials were performed for each mouse during each time point, which were then averaged. The mean and SD of the three trials for each mouse's motor parameters were analyzed.

For the serum Hex A activity assay analysis, two analyses were performed: (1) 2-way ANOVA with Tukey's multiple comparisons to test statistical significance seen within each time point and (2) 1-way ANOVA with Tukey's multiple comparisons to test the individual cohorts statistical significance across time points. Hex A activity was measured until each cohort had 3 mice surviving. For the MB, CB, and liver Hex A assay analysis, a 1-way ANOVA was used with Tukey's post hoc analysis for multiple pairwise comparisons.

The GM2 assay was analyzed in terms of density of GM2/GD1a bands for each dose group. A 1-way ANOVA with Tukey's multiple comparisons was used to compare the GM2/GD1a value across dose groups. Next, the vector biodistribution was measured with regard to vector genome/mouse genome within each organ. A 2-way ANOVA and Tukey's multiple comparisons were used to compare vector biodistribution across all the organs and dose groups. The Kaplan-Meier survival curve was analyzed with a log rank (Mantel-Cox) test to assess significant differences in dose-dependent survival.

For all statistical analyses, the α value was set for 0.05, such that a p value <0.05 was considered to indicate statistical significance.

DATA AND CODE AVAILABILITY

All data are provided with this report. Raw datasets generated for statistical analysis of the present study are available from Dr. Walia upon reasonable request.

SUPPLEMENTAL INFORMATION

Supplemental information can be found online at https://doi.org/10.1016/j.omtm.2023.101168.

ACKNOWLEDGMENTS

Funding for this research was provided by Cure Tay-Sachs Foundation and GlycoNet.

AUTHOR CONTRIBUTIONS

A.E.R. performed all injections, daily gavage, blood collections, behavioral testing, humane endpoint tissue harvesting, all experiments, and statistical analysis and wrote the initial manuscript draft. N.M.D. assisted in tissue harvesting at endpoints, some behavioral testing, and blood collections, and gavage. B.M.Q. also assisted during necropsy, and some gavage. M.M. performed all breeding and maintaining of the *Hexb* colony for this project and assisted with gavage and necropsy. Z.C. provided help with qPCR experimentation and analysis. K.J.L.O. did the analysis of the Hex data for the MB and the lifespan body weights and helped with data analysis for all outcome measures. S.J.G. advised on the initial study design and edited the manuscript. J.S.W. supervised all aspects of the project.

DECLARATION OF INTERESTS

The authors declare no competing interests.

REFERENCES

1. Conzelmann, E., and Sandhoff, K. (1983). Partial enzyme deficiencies: residual activities and the development of neurological disorders. Dev. Neurosci. *6*, 58–71.
2. Andersson, U., Smith, D., Jeyakumar, M., Butters, T.D., Borja, M.C., Dwek, R.A., and Platt, F.M. (2004). Improved outcome of N-butyldeoxygalactonojirimycin-mediated substrate reduction therapy in a mouse model of Sandhoff disease. Neurobiol. Dis. *16*, 506–515.
3. Jeyakumar, M., Butters, T.D., Cortina-Borja, M., Hunnam, V., Proia, R.L., Perry, V.H., Dwek, R.A., and Platt, F.M. (1999). Delayed symptom onset and increased life expectancy in Sandhoff disease mice treated with N-butyldeoxynojirimycin. Proc. Natl. Acad. Sci. USA *96*, 6388–6393.
4. Chiricozzi, E., Niemir, N., Aureli, M., Magini, A., Loberto, N., Prinetti, A., Bassi, R., Polchi, A., Emiliani, C., Caillaud, C., and Sonnino, S. (2014). Chaperone therapy for GM2 gangliosidosis: effects of pyrimethamine on β-hexosaminidase activity in Sandhoff fibroblasts. Mol. Neurobiol. *50*, 159–167.
5. Maegawa, G.H.B., Tropak, M., Buttner, J., Stockley, T., Kok, F., Clarke, J.T.R., and Mahuran, D.J. (2007). pyrimethamine as a potential pharmacological chaperone for late-onset forms of GM_2 gangliosidosis. J. Biol. Chem. *282*, 9150–9161.
6. Matsuoka, K., Tsuji, D., Aikawa, S.I., Matsuzawa, F., Sakuraba, H., and Itoh, K. (2010). Introduction of an N-glycan sequon into HEXA enhances human beta-hexosaminidase cellular uptake in a model of Sandhoff disease. Mol. Ther. *18*, 1519–1526.
7. Tsuji, D., Akeboshi, H., Matsuoka, K., Yasuoka, H., Miyasaki, E., Kasahara, Y., Kawashima, I., Chiba, Y., Jigami, Y., Taki, T., et al. (2011). Highly phosphomannosylated enzyme replacement therapy for GM2 gangliosidosis. Ann. Neurol. *69*, 691–701.
8. Clarke, J.T.R., Mahuran, D.J., Sathe, S., Kolodny, E.H., Rigat, B.A., Raiman, J.A., and Tropak, M.B. (2011). An open-label Phase I/II clinical trial of pyrimethamine for the treatment of patients affected with chronic GM2 gangliosidosis (Tay–Sachs or Sandhoff variants). Mol. Genet. Metabol. *102*, 6–12.
9. Jacobs, J.F.M., Willemsen, M.a. a.P., Groot-Loonen, J.J., Wevers, R.A., and Hoogerbrugge, P.M. (2005). Allogeneic BMT followed by substrate reduction therapy in a child with subacute Tay-Sachs disease. Bone Marrow Transplant. *36*, 925–926.
10. Maegawa, G.H.B., van Giersbergen, P.L.M., Yang, S., Banwell, B., Morgan, C.P., Dingemanse, J., Tifft, C.J., and Clarke, J.T.R. (2009). Pharmacokinetics, safety and tolerability of miglustat in the treatment of pediatric patients with GM2 gangliosidosis. Mol. Genet. Metabol. *97*, 284–291.
11. Maegawa, G.H.B., Banwell, B.L., Blaser, S., Sorge, G., Toplak, M., Ackerley, C., Hawkins, C., Hayes, J., and Clarke, J.T.R. (2009). Substrate reduction therapy in juvenile GM2 gangliosidosis. Mol. Genet. Metabol. *98*, 215–224.
12. Osher, E., Fattal-Valevski, A., Sagie, L., Urshanski, N., Sagiv, N., Peleg, L., Lerman-Sagie, T., Zimran, A., Elstein, D., Navon, R., et al. (2015). Effect of cyclic, low dose pyrimethamine treatment in patients with Late Onset Tay Sachs: an open label, extended pilot study. Orphanet J. Rare Dis. *10*, 45.
13. Prasad, V.K., Mendizabal, A., Parikh, S.H., Szabolcs, P., Driscoll, T.A., Page, K., Lakshminarayanan, S., Allison, J., Wood, S., Semmel, D., et al. (2008). Unrelated donor umbilical cord blood transplantation for inherited metabolic disorders in 159 pediatric patients from a single center: influence of cellular composition of the graft on transplantation outcomes. Blood *112*, 2979–2989.
14. Shapiro, B.E., Pastores, G.M., Gianutsos, J., Luzy, C., and Kolodny, E.H. (2009). Miglustat in late-onset Tay-Sachs disease: a 12-month, randomized, controlled clinical study with 24 months of extended treatment. Genet. Med. *11*, 425–433.
15. Arfi, A., Bourgoin, C., Basso, L., Emiliani, C., Tancini, B., Chigorno, V., Li, Y.T., Orlacchio, A., Poenaru, L., Sonnino, S., and Caillaud, C. (2005). Bicistronic lentiviral vector corrects β-hexosaminidase deficiency in transduced and cross-corrected human Sandhoff fibroblasts. Neurobiol. Dis. *20*, 583–593.
16. Cachón-González, M.B., Wang, S.Z., Lynch, A., Ziegler, R., Cheng, S.H., and Cox, T.M. (2006). Effective gene therapy in an authentic model of Tay-Sachs-related diseases. Proc. Natl. Acad. Sci. USA *103*, 10373–10378.
17. Guidotti, J.E., Mignon, A., Haase, G., Caillaud, C., McDonell, N., Kahn, A., and Poenaru, L. (1999). Adenoviral Gene Therapy of the Tay-Sachs Disease in Hexosaminidase A-Deficient Knock-Out Mice. Hum. Mol. Genet. *8*, 831–838.
18. Karumuthil-Melethil, S., Nagabhushan Kalburgi, S., Thompson, P., Tropak, M., Kaytor, M.D., Keimel, J.G., Mark, B.L., Mahuran, D., Walia, J.S., and Gray, S.J. (2016). Novel Vector Design and Hexosaminidase Variant Enabling Self-Complementary Adeno-Associated Virus for the Treatment of Tay-Sachs Disease. Hum. Gene Ther. *27*, 509–521.
19. Martino, S., Marconi, P., Tancini, B., Dolcetta, D., De Angelis, M.G.C., Montanucci, P., Bregola, G., Sandhoff, K., Bordignon, C., Emiliani, C., et al. (2005). A direct gene transfer strategy via brain internal capsule reverses the biochemical defect in Tay–Sachs disease. Hum. Mol. Genet. *14*, 2113–2123.
20. Ornaghi, F., Sala, D., Tedeschi, F., Maffia, M.C., Bazzucchi, M., Morena, F., Valsecchi, M., Aureli, M., Martino, S., and Gritti, A. (2020). Novel bicistronic lentiviral vectors correct β-Hexosaminidase deficiency in neural and hematopoietic stem cells and progeny: implications for *in vivo* and ex vivo gene therapy of GM2 gangliosidosis. Neurobiol. Dis. *134*, 104667.
21. Osmon, K.J.L., Woodley, E., Thompson, P., Ong, K., Karumuthil-Melethil, S., Keimel, J.G., Mark, B.L., Mahuran, D., Gray, S.J., and Walia, J.S. (2016). Systemic Gene Transfer of a Hexosaminidase Variant Using an scAAV9.47 Vector Corrects GM2 Gangliosidosis in Sandhoff Mice. Hum. Gene Ther. *27*, 497–508.
22. Tropak, M.B., Yonekawa, S., Karumuthil-Melethil, S., Thompson, P., Wakarchuk, W., Gray, S.J., Walia, J.S., Mark, B.L., and Mahuran, D. (2016). Construction of a hybrid β-hexosaminidase subunit capable of forming stable homodimers that hydrolyze GM2 ganglioside *in vivo*. Mol. Ther. Methods Clin. Dev. *3*, 15057.
23. Woodley, E., Osmon, K.J.L., Thompson, P., Richmond, C., Chen, Z., Gray, S.J., and Walia, J.S. (2019). Efficacy of a Bicistronic Vector for Correction of Sandhoff Disease in a Mouse Model. Mol. Ther. Methods Clin. Dev. *12*, 47–57.
24. Vannucci, L., Lai, M., Chiuppesi, F., Ceccherini-Nelli, L., and Pistello, M. (2013). Viral vectors: a look back and ahead on gene transfer technology. New Microbiol. *36*, 1–22.
25. Flotte, T.R., Cataltepe, O., Puri, A., Batista, A.R., Moser, R., McKenna-Yasek, D., Douthwright, C., Gernoux, G., Blackwood, M., Mueller, C., et al. (2022). AAV gene therapy for Tay-Sachs disease. Nat. Med. *28*, 251–259.
26. Liu, Z., Chen, O., Wall, J.B.J., Zheng, M., Zhou, Y., Wang, L., Vaseghi, H.R., Qian, L., and Liu, J. (2017). Systematic comparison of 2A peptides for cloning multi-genes in a polycistronic vector. Sci. Rep. *7*, 2193.
27. Blanchette, M., and Daneman, R. (2015). Formation and maintenance of the BBB. Mech. Dev. *138*, 8–16.
28. Saunders, N.R., Dreifuss, J.J., Dziegielewska, K.M., Johansson, P.A., Habgood, M.D., Møllgård, K., and Bauer, H.C. (2014). The rights and wrongs of blood-brain barrier permeability studies: a walk through 100 years of history. Front. Neurosci. *8*, 404.

29. Kirkegaard, T., Gray, J., Priestman, D.A., Wallom, K.L., Atkins, J., Olsen, O.D., Klein, A., Drndarski, S., Petersen, N.H.T., Ingemann, L., et al. (2016). Heat Shock Protein-based therapy as a potential candidate for treating sphingolipidoses. Sci. Transl. Med. *8*, 355ra118.

30. Hinderer, C., Bell, P., Katz, N., Vite, C.H., Louboutin, J.P., Bote, E., Yu, H., Zhu, Y., Casal, M.L., Bagel, J., et al. (2018). Evaluation of Intrathecal Routes of Administration for Adeno-Associated Viral Vectors in Large Animals. Hum. Gene Ther. *29*, 15–24.

31. Hocquemiller, M., Giersch, L., Audrain, M., Parker, S., and Cartier, N. (2016). Adeno-Associated Virus-Based Gene Therapy for CNS Diseases. Hum. Gene Ther. *27*, 478–496.

32. McCurdy, V.J., Rockwell, H.E., Arthur, J.R., Bradbury, A.M., Johnson, A.K., Randle, A.N., Brunson, B.L., Hwang, M., Gray-Edwards, H.L., Morrison, N.E., et al. (2015). Widespread correction of central nervous system disease after intracranial gene therapy in a feline model of Sandhoff disease. Gene Ther. *22*, 181–189.

33. Tropak, M.B., Reid, S.P., Guiral, M., Withers, S.G., and Mahuran, D. (2004). Pharmacological Enhancement of β-Hexosaminidase Activity in Fibroblasts from Adult Tay-Sachs and Sandhoff Patients. J. Biol. Chem. *279*, 13478–13487.

34. Tropak, M.B., Blanchard, J.E., Withers, S.G., Brown, E.D., and Mahuran, D. (2007). High-Throughput Screening for Human Lysosomal β-N-Acetyl Hexosaminidase Inhibitors Acting as Pharmacological Chaperones. Chem. Biol. *14*, 153–164.

35. Niemir, N., Rouvière, L., Besse, A., Vanier, M.T., Dmytrus, J., Marais, T., Astord, S., Puech, J.P., Panasyuk, G., Cooper, J.D., et al. (2018). Intravenous administration of scAAV9-Hexb normalizes lifespan and prevents pathology in Sandhoff disease mice. Hum. Mol. Genet. *27*, 954–968.

36. Walia, J.S., Altaleb, N., Bello, A., Kruck, C., LaFave, M.C., Varshney, G.K., Burgess, S.M., Chowdhury, B., Hurlbut, D., Hemming, R., et al. (2015). Long-Term Correction of Sandhoff Disease Following Intravenous Delivery of rAAV9 to Mouse Neonates. Mol. Ther. *23*, 414–422.

37. Chen, X., Dong, T., Hu, Y., De Pace, R., Mattera, R., Eberhardt, K., Ziegler, M., Pirovolakis, T., Sahin, M., Bonifacino, J.S., et al. (2023). Intrathecal AAV9/AP4M1 gene therapy for hereditary spastic paraplegia 50 shows safety and efficacy in preclinical studies. J. Clin. Invest. *133*, e164575.

38. Chen, X., Snanoudj-Verber, S., Pollard, L., Hu, Y., Cathey, S.S., Tikkanen, R., and Gray, S.J. (2021). Pre-clinical Gene Therapy with AAV9/AGA in Aspartylglucosaminuria Mice Provides Evidence for Clinical Translation. Mol. Ther. *29*, 989–1000.

39. Chen, X., Dong, T., Hu, Y., Shaffo, F.C., Belur, N.R., Mazzulli, J.R., and Gray, S.J. (2022). AAV9/MFSD8 gene therapy is effective in preclinical models of neuronal ceroid lipofuscinosis type 7 disease. J. Clin. Invest. *132*, e146286.

40. Chen, X., Lim, D.A., Lawlor, M.W., Dimmock, D., Vite, C.H., Lester, T., Tavakkoli, F., Sadhu, C., prasad, S., and Gray, S.J. (2023). Biodistribution of Adeno-Associated Virus Gene Therapy Following Cerebrospinal Fluid-Directed Administration. Hum. Gene Ther. *34*, 94–111.

41. Kot, S., Karumuthil-Melethil, S., Woodley, E., Zaric, V., Thompson, P., Chen, Z., Lykken, E., Keimel, J.G., Kaemmerer, W.F., Gray, S.J., and Walia, J.S. (2021). Investigating Immune Responses to the scAAV9-HEXM Gene Therapy Treatment in Tay-Sachs Disease and Sandhoff Disease Mouse Models. Int. J. Mol. Sci. *22*, 6751.

42. Castelli, V., Benedetti, E., Antonosante, A., Catanesi, M., Pitari, G., Ippoliti, R., Cimini, A., and d'Angelo, M. (2019). Neuronal Cells Rearrangement During Aging and Neurodegenerative Disease: Metabolism, Oxidative Stress and Organelles Dynamic. Front. Mol. Neurosci. *12*, 132.

43. Ryckman, A.E., Brockhausen, I., and Walia, J.S. (2020). Metabolism of Glycosphingolipids and Their Role in the Pathophysiology of Lysosomal Storage Disorders. Int. J. Mol. Sci. *21*, E6881.

44. Szymanska, H., Lechowska-Piskorowska, J., Krysiak, E., Strzalkowska, A., Unrug-Bielawska, K., Grygalewicz, B., Skurzak, H.M., Pienkowska-Grela, B., and Gajewska, M. (2014). Neoplastic and Nonneoplastic Lesions in Aging Mice of Unique and Common Inbred Strains Contribution to Modeling of Human Neoplastic Diseases. Vet. Pathol. *51*, 663–679.

45. Chandler, R.J., LaFave, M.C., Varshney, G.K., Trivedi, N.S., Carrillo-Carrasco, N., Senac, J.S., Wu, W., Hoffmann, V., Elkahloun, A.G., Burgess, S.M., and Venditti, C.P. (2015). Vector design influences hepatic genotoxicity after adeno-associated virus gene therapy. J. Clin. Invest. *125*, 870–880.

46. Donsante, A., Miller, D.G., Li, Y., Vogler, C., Brunt, E.M., Russell, D.W., and Sands, M.S. (2007). AAV vector integration sites in mouse hepatocellular carcinoma. Science *317*, 477.

47. Bell, P., Wang, L., Lebherz, C., Flieder, D.B., Bove, M.S., Wu, D., Gao, G.P., Wilson, J.M., and Wivel, N.A. (2005). No evidence for tumorigenesis of AAV vectors in a large-scale study in mice. Mol. Ther. *12*, 299–306.

48. Li, H., Malani, N., Hamilton, S.R., Schlachterman, A., Bussadori, G., Edmonson, S.E., Shah, R., Arruda, V.R., Mingozzi, F., Wright, J.F., et al. (2011). Assessing the potential for AAV vector genotoxicity in a murine model. Blood *117*, 3311–3319.

49. Shaimardanova, A.A., Chulpanova, D.S., Solovyeva, V.V., Aimaletdinov, A.M., and Rizvanov, A.A. (2022). Functionality of a bicistronic construction containing HEXA and HEXB genes encoding β-hexosaminidase A for cell-mediated therapy of GM2 gangliosidoses. Neural Regen. Res. *17*, 122–129.

50. Osmon, K.J., Thompson, P., Woodley, E., Karumuthil-Melethil, S., Heindel, C., Keimel, J.G., Kaemmerer, W.F., Gray, S.J., and Walia, J.S. (2022). Treatment of GM2 Gangliosidosis in Adult Sandhoff Mice Using an Intravenous Self-Complementary Hexosaminidase Vector. Curr. Gene Ther. *22*, 262–276.

51. Jones, C.P., Boyd, K.L., and Wallace, J.M. (2016). Evaluation of Mice Undergoing Serial Oral Gavage While Awake or Anesthetized. J. Am. Assoc. Lab. Anim. Sci. *55*, 805–810.

52. Arantes-Rodrigues, R., Henriques, A., Pinto-Leite, R., Faustino-Rocha, A., Pinho-Oliveira, J., Teixeira-Guedes, C., Seixas, F., Gama, A., Colaço, B., Colaço, A., and Oliveira, P.A. (2012). The effects of repeated oral gavage on the health of male CD-1 mice. Lab. Anim *41*, 129–134.

53. Walker, M.K., Boberg, J.R., Walsh, M.T., Wolf, V., Trujillo, A., Duke, M.S., Palme, R., and Felton, L.A. (2012). A less stressful alternative to oral gavage for pharmacological and toxicological studies in mice. Toxicol. Appl. Pharmacol. *260*, 65–69.

54. Kinghorn, K.J., Grönke, S., Castillo-Quan, J.I., Woodling, N.S., Li, L., Sirka, E., Gegg, M., Mills, K., Hardy, J., Bjedov, I., and Partridge, L. (2016). A Drosophila Model of Neuronopathic Gaucher Disease Demonstrates Lysosomal-Autophagic Defects and Altered mTOR Signalling and Is Functionally Rescued by Rapamycin. J. Neurosci. *36*, 11654–11670.

55. Boland, B., Kumar, A., Lee, S., Platt, F.M., Wegiel, J., Yu, W.H., and Nixon, R.A. (2008). Autophagy Induction and Autophagosome Clearance in Neurons: Relationship to Autophagic Pathology in Alzheimer's Disease. J. Neurosci. *28*, 6926–6937.

56. Bailey, R.M., Rozenberg, A., and Gray, S.J. (2020). Comparison of high-dose intracisterna magna and lumbar puncture intrathecal delivery of AAV9 in mice to treat neuropathies. Brain Res. *1739*, 146832.

57. Gray, S.J., Nagabhushan Kalburgi, S., McCown, T.J., and Jude Samulski, R. (2013). Global CNS Gene Delivery and Evasion of Anti-AAV Neutralizing Antibodies by Intrathecal AAV Administration in Non-Human Primates. Gene Ther. *20*, 450–459.

58. Phaneuf, D., Wakamatsu, N., Huang, J.Q., Borowski, A., Peterson, A.C., Fortunato, S.R., Ritter, G., Igdoura, S.A., Morales, C.R., Benoit, G., et al. (1996). Dramatically Different Phenotypes in Mouse Models of Human Tay-Sachs and Sandhoff Diseases. Hum. Mol. Genet. *5*, 1–14.

59. Osmon, K.J., Vyas, M., Woodley, E., Thompson, P., and Walia, J.S. (2018). Battery of Behavioral Tests Assessing General Locomotion, Muscular Strength, and Coordination in Mice. J. Vis. Exp. *131*, 55491.

60. Wherrett, J., and Cumings, J. (1963). Detection and resolution of gangliosides in lipid extracts by thin-layer chromatography. Biochem. J. *86*, 378–382.

61. Folch, J., Lees, M., and Sloane Stanley, G.H. (1957). A simple method for the isolation and purification of total lipides from animal tissues. J. Biol. Chem. *226*, 497–509.